Compact Self-Supportive Filters Suitable for Additive Manufacturing

Mostaani, Abolfazl; Wang, Yi; Qian, Lu; Mohamed, Abd el-Moez a.; Attallah, Moataz m.; Skaik, Talal

DOI:
10.1109/TCPMT.2023.3332678

Compact Self-Supportive Filters Suitable for Additive Manufacturing

Abolfazl Mostaani, Yi Wang, *Senior Member, IEEE*, Lu Qian, *Graduate Student Member, IEEE*, Abd El-Moez A. Mohamed, Moataz M. Attallah, and Talal Skaik

***Abstract*—An irregular-hexagonal resonator geometry is proposed for additively manufactured microwave filters. This geometry allows closely packed resonators to form very compact filters of various topologies fulfilling transfer functions with transmission zeros. It also minimizes the overhangs and allows vertical printing along the direction of the input/output ports, without any internal support structure and with a much-reduced profile. The characteristics of the resonator and the trade-off between compactness and quality factor has been analyzed. Three bandpass filters have been demonstrated. Two of them are designed with non-resonating node topologies with fractional bandwidths of 5% and 1%, respectively, using the step-tuning technique. All three filters are fabricated using selective laser melting (SLM) technique. The performance of the fabricated filters is compared with the EM simulation. Very good agreement has been achieved for all three filters. The effectiveness of tuning has also been demonstrated. The resonator structure has offered high printability in the manufacturing and high level of modularity and flexibility in the design.**

***Index Terms*— Bandpass filter (BPF), coupling matrix, microwave filter, non-resonating node, transmission zeros, 3-D printing.**

II. Introduction

The emergence of additive manufacturing (AM, also known as 3D-printing) was a turning point in the manufacturing industries due to its unique capability of building complex structures with reduced need of assembly or even in one piece. In microwave engineering, AM offers a promising solution to the increasing demand for more compact, complex and lighter structures, especially in satellite communicating systems. One widely used device that has benefited most from the new manufacturing technique is the filter. In recent years, there have been numerous studies on high performance filters and multiplexers fabricated using various AM technologies such as fused deposition modeling (FDM) [1],[2], polyjet printing [3], stereolithographic apparatus (SLA) [4],[5] and selective laser melting (SLM) [6]-[10].

While 3D printing brings about many innovation opportunities in filter design and manufacture, it is not a technology without challenges. The printability and the printing quality are highly dependent on the relationship between the geometry and printing direction. Fig. 1 illustrates the formation of the internal surfaces, which often concern microwave parts most, from the layer-by-layer manufacture process using the SLM as an example. The staircase effect makes the 3D printed surfaces much rougher than machined surfaces. The up-skin areas face along the printing direction, whereas the down-skin areas face against the printing direction. The down-skin surfaces form on un-sintered powder in SLM so they have higher surface roughness. These are also referred to as the overhang, described by the angle θ_d. To ensure the integrity of the structure, this angle should normally be kept below 45° [11]. The larger the overhang angle is, the rougher the down-skin surface will be. For microwave filters where surface roughness significantly impacts the insertion loss, θ_d is preferred to be less than 30°. The region marked out as 'E' in Fig. 1, with large overhang angles, should really be avoided. The region B, with a large angle θ_u but in the up-skin area, can be readily formed with good quality but the staircase effect would make the hatch pattern of the laser visible on the surface. One of the main considerations in designing such filters for 3D printing is to

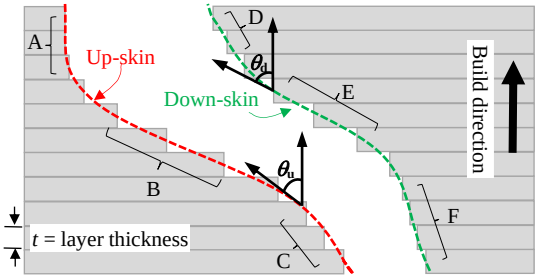

Fig. 1. An illustration of the surface texture/roughness in relation to build orientation, θ_u and θ_d, for the up-skin and down-skin surfaces.

Fig. 2. Some typical self-supportive cavity structures used in 3D printing.

This work is supported by the UK Engineering and Physical Science Research Council under grant EP/S013113/1. (Corresponding author: Y. Wang)

A. Mostaani, Y. Wang, L. Qian, and T. Skaik are with the School of Engineering University of Birmingham, Birmingham B15 2TT, U.K. (e-mail: axm1637@student.bham.ac.uk; y.wang.1@bham.ac.uk; lxq961@student.bham.ac.uk; T.F.Skaik@bham.ac.uk;).

Abd El-Moez A. Mohamed and Moataz M. Attallah are with the School of Metallurgy and Materials, University of Birmingham, Birmingham B15 2TT, U.K. (e-mail: a.a.m.a.hussein@bham.ac.uk; m.m.attallah@bham.ac.uk).

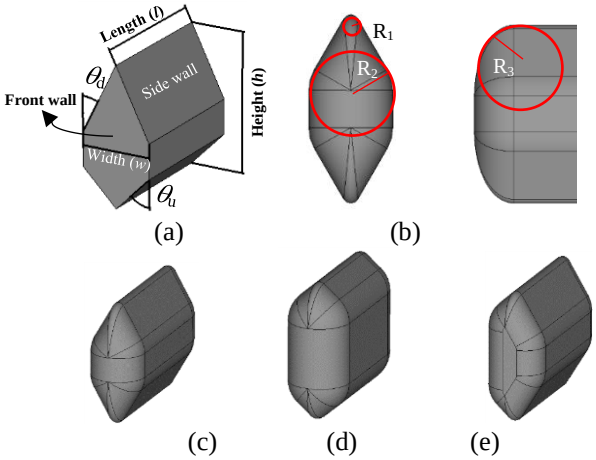

Fig. 3. (a) Primary and (b) modified model of the proposed resonator. (c), (d), (e): Three types of resonators with varying θ_d of 30˚, 45˚ and mixed 30˚/45˚.

avoid or minimize the overhang problems, avoid excessive surface roughness and therefore reduce the risk of structural failure or significant performance degradation [12]-[15]. This makes self-supportive geometries highly desirable for cavity resonators/filters. Some of these geometries can be found in Fig. 2. The rounded structures are good choice. But the north-pole area may be modified to avoid any flat ceiling structure. The self-supportive geometries also give the opportunity to design filters to be printed vertically, which saves footprint on the printing platform for more parts to be printed in one go. One caveat is the moderately increased risk in building tall structures when instability of the printer platform during long print could disrupt or fail the parts. So, it is often desirable to design the structures as compact as possible in both scanning (horizontal) and printing (vertical) directions. In [16], a filter based on spherical resonators is printed vertically using SLM technology. The resonators are stacked upon each other. The ceiling of the spheres is removed to create the coupling irises while avoiding overhangs. If the spheres are staggered sideway, the pole ceiling may have to be modified. The triangular resonator [17] is good for printing but not the most suitable for stacking up. Conventional rectangular resonators must be tilted in printing, e.g., by 45˚ [10]. The rhombus shape resonator with θ_d < 45˚ offers a good balance in the printability, internal surface finishing and flexibility to create a compact stack and layout. The adjacent resonators can be attached diagonally rather than on top of each other. As with the triangular shape, it has sharp corners which may present some difficulties with surface coating, if required.

In this paper an irregular-hexagon shaped resonator is proposed and used. This structure reduces the overhangs and enhance the printability and modularity of the filters. The geometry allows closely packed resonators laid out in a low profile and in various topologies to realize transmission zeros in the transfer function. It also enables the filters to be printed in a vertical sitting direction along the direction of the ports, without requiring any internal support structures and without the need of tilting the build as in many rectangular cavity-based filters. The resonator structures and the filters formed of them

TABLE I
RESONANT FREQUENCY AND Q_U COMPARISON BETWEEN THE PROPOSED RESONATORS AND RECTANGULAR RESONATOR

	Resonant frequency (GHz) / Q_u			
θ_d	30˚	45˚	30˚/45˚	Rec.
Mode 1	10/7007	10/8562	10/7848	10/7794
Mode 2	13.1/9153	14.9/10865	15/9850	15.1/9749

are highly suitable for 3D printing. The paper is organized as follows: Section II explains the proposed resonator and its characteristics. This is followed by three design examples, including the design method, and their verification results, before the conclusions.

II. RESONATOR GEOMETRY

First, we will introduce the self-supportive resonator structure for 3D printing. Fig. 3(a) shows the primary model of the resonator. The resonator side walls are narrowing towards the ceiling at a slope angle, θ_d against the vertical axis. This angle is adjustable but preferentially set at 30˚ to reduce the risk of overhang-associated excessive surface roughness [18]. The side walls are also narrowing at an angle of θ_u towards the bottom of the resonator. This angle can be more flexibly chosen but set to be equal to θ_d in order to create a symmetric geometry. Similar resonator is presented in [19], in which the resonators not only have sharp corners but also stack on top of each other. In this paper, the sharp corners are rounded, and the resonators are staggered to make a very compact layout and to realize transmission zeros using dangling nodes, while still being printed vertically with minimum overhang. Fig. 3(b) shows the resonator with corners rounded by R_1=1 mm, R_2=5 mm and R_3=5.08 mm. The modified resonator structure is shown in Fig. 3(c). Its Q_u for the first two modes is compared with two other variations (with different θ_d values) and the rectangular resonator in Table I. All resonators are designed to have their fundamental resonant mode at 10 GHz. The Q_u of the proposed resonator with θ_d = 30˚ is 10% lower than the rectangular resonator. The lower Q_u could be caused by the fact that the 60˚ side wall slope (θ_d = 30˚) creates sharper sides in the cavity. This confines the field and increases the current density. This reduces the efficiency of the resonator and lead to a lower Q_u factor compared to cavity resonators with smooth, rounded geometries. The sharp corners in a cavity resonator can also encourage the excitation of higher-order modes in the resonator. The volume and length of the resonator is also 4.8% and 66% bigger than the rectangular version, respectively. The Q_u can be increased by increasing the θ_d to 45˚ (Fig. 3(d)). However, this would reduce the finishing quality of the internal downward surfaces. It would also increase the total height of the filters, which may be unfavorable as the increased printing height also means more powder to fill the printer tank as well as increased risk of instability. A resonator with a mixed θ_d of 30˚ and 45˚ (Fig. 3(e)) could offer slightly higher Q_u than the rectangular resonator. This geometry may be suitable for inline filters but

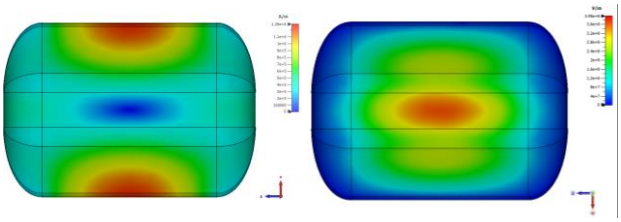

(a) (b)

Fig. 4. Field patterns of the proposed hexagonal resonator with $\theta_d = \theta_u = 30^\circ$. (a) H-field. (b) E-field.

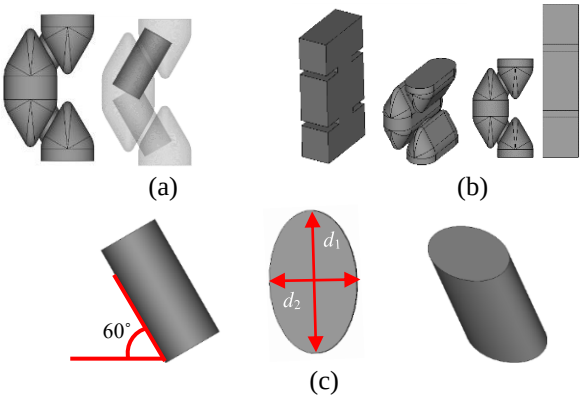

(a) (b) (c)

Fig. 5. A single resonator and the coupling structure. (a) Side view. (b) Comparison with a rectangular resonator that has the same resonance frequency and loaded Q. (c) The elliptical iris structure.

becomes inconvenient when dangling resonators are used. On balance, we have adopted θ_d as 30˚ for the resonators in the designs. Its electrical and magnetic fields patterns are displayed in Fig. 4. Fig. 5(a) and (b) show a single resonator coupled to two ports and is compared with its counterpart rectangular resonator. An elliptic coupling iris is used as shown in Fig. 5(c). The coupling can be adjusted by changing the major and minor axes of the ellipse. The ports are based on WR90 waveguide. For both source and load irises, d_1 and d_2 are 9.8 mm and 6 mm, respectively. For the hexagonal resonator, l is 28 mm. h and w are equal to the standard WR90 waveguide, i.e., 22.86 mm and 10.16 mm, respectively. For the regular rectangular resonator, h is 16.9 mm. The rest of the dimensions are based on WR90. The source and load irises' length and width are 8.9 mm and 10.16 mm, respectively. The proposed resonator has a higher cut-off frequency, but slightly lower second-order mode frequency compared with the rectangular resonator. The compactness of the hexagonal resonator is evident as shown in Fig. 5(b). The resonator can be printed vertically, unlike the conventional rectangular resonators, which must be printed with a 45˚ tilt. Cross-coupling extracted pole and non-resonating nodes can all be implemented using the proposed resonator model. In this paper, the non-resonating node designs have been chosen.

III. Filter Design and Results

Three bandpass filters, narrowband and wideband, have been designed and fabricated to demonstrate the capability of the proposed resonators over the rectangular resonators. They are fabricated with aluminum-copper alloy (A20X) using Concept Laser M2 based on selective laser melting (SLM) printing technology. The fabricated filters are polished using vibratory grinding machine to reduce the surface roughness. The measured typical surface roughness and the nominal electrical conductivity of A20X are around 3.5 μm and 1.9×10^7 S/m, respectively. These are used to obtain the effective conductivity, which is around 0.56×10^7 S/m and used in the simulations to obtain insertion loss. The first and second designs are a third-order filter each with two transmission zeros realized using dangling nodes. The filters are different in their bandwidth (1% and 5% FBW) and topology. Both filters have been designed using the non-resonating node method [20], [21]. The third design is a third-order Chebyshev filter.

A. A third-order wideband filter with two transmission zeros

Fig. 6 shows a third-order filter topology with two transmission zeros (TZs) together with its equivalent circuit model. The specification of the filter is: f_c = 10 GHz, BW = 500 MHz, Return loss (RL) = 20 dB, and TZs at 9.25 GHz and 10.75 GHz. The filter is synthesised using the non-resonating node method and the values of circuit elements in Fig. 6(b) are obtained as J_1 = 1, J_2 = 2.5285, J_3 = 1, J_4 = 2.8878, J_5 = 1.1078, J_6 = 1.0685, b_1 = 2.0154j, b_2 = 3j, b_3 = -3.1887j, b_4 = -3j and b_5 = -0.3411j. All the capacitances are normalized to 1. The coupling matrix is acquired from the circuit elements and presented in (1).

$$\begin{bmatrix} 0.0000 & 1.0000 & 0.0000 & 0.0000 & 0.0000 & 0.0000 & 0.0000 \\ 1.0000 & 2.0154 & 2.5285 & 1.0000 & 0.0000 & 0.0000 & 0.0000 \\ 0.0000 & 2.5285 & 3.0000 & 0.0000 & 0.0000 & 0.0000 & 0.0000 \\ 0.0000 & 1.0000 & 0.0000 & -3.189 & 2.8878 & 1.1078 & 0.0000 \\ 0.0000 & 0.0000 & 0.0000 & 2.8878 & -3.000 & 0.0000 & 0.0000 \\ 0.0000 & 0.0000 & 0.0000 & 1.1078 & 0.0000 & -0.341 & 1.0685 \\ 0.0000 & 0.0000 & 0.0000 & 0.0000 & 0.0000 & 1.0685 & 0.0000 \end{bmatrix} \quad (1)$$

The filter is designed using the step-tuning technique [10], in which the filter's topology is divided to three subsections (Fig. 6(a)), whose corresponding coupling matrices are extracted from the main coupling matrix in (1). Fig. 7 shows the three subsections and their coupling matrix. Each subsection is designed separately by optimization so that its S-parameters match those from the corresponding coupling submatrix. It must be noted that, in each subsection, one or two internal couplings must be converted to external couplings. For example, in the case of Fig. 7(b), the internal couplings J_3 and J_5 in Fig. 6(a) are converted to the external coupling J_3' and J_5' using the following equation [10]:

$$J_i' = J_i \times \sqrt{FBW \frac{\pi}{2}\left(\frac{\lambda_g}{\lambda}\right)^2} \quad (2)$$

where J_i' represents the external coupling of the submatrix, J_i is the internal coupling of the coupling matrix, λ and λ_g are the free-space and guided wavelength, respectively. The diagonal elements of the submatrix, representing the self-coupling (for resonators, NRNs or ports), are also adjusted. For example, in the case of Fig. 7(b), the diagonal elements corresponding to S and L are set to zero. Similar process is applied to other subsections. EM design for each subsection is achieved by

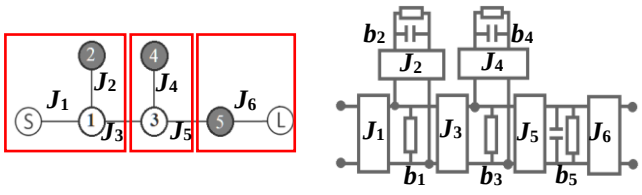

(a) (b)

Fig. 6. A third-order filter with two transmission zeros. (a) Topology, which is divided into three subsections using three red rectangles. Dark and white circles represent resonators and NRNs, respectively. (b) Equivalent circuit model.

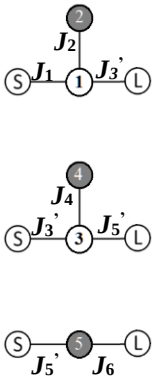

	S	1	2	L
S	0	1	0	0
1	1	2.0154	2.5285	0.3713
2	0	2.5285	3	0
L	0	0.3713	0	0

(a)

	S	1	2	L
S	0	0.3713	0	0
1	0.3713	-3.189	2.8878	0.411
2	0	2.8878	-3	0
L	0	0.4114	0	0

(b)

	S	3	L
S	0	0.4114	0
3	0.4114	-0.341	1.0685
L	0	1. 0685	0

(c)

Fig. 7. The three subsections of the filter. (a) First subsection including NRN 1 and resonator 2. J_3 is changed to J_3' using (2). (b) Second subsection including the NRN 3 and resonator 4. (c) Last subsection.

dimensioning and optimization to fulfil the S-parameters of the submatrix. For the dimensioning process, the values of R_1, R_2, R_3 (for resonators) and minor axis (for irises) are fixed as defined in Section II. The only two parameters that control the resonant frequency and the coupling are l and the major axis, respectively. By controlling the value of l and the major axis, each subsection is designed to match the corresponding coupling matrix frequency response. Finally, all the subsections are joined together and optimized. Fig. 8 shows the filter based on an E-plane configuration, using WR90 waveguide. The dominant mode is TE101. The designed structure can be seen in Fig. 8(a). The filter has been designed with 5×M2 tuning screws on the side wall (see Fig. 3(a)) of each resonator and the NRN to fix the frequency detuning. The screws are designed to be inside each cavity by half of the cavity's length. The dimensions of the filter are as follows: d_{S1} (major axis of the elliptical iris between source and resonator 1) = 16.02 mm, d_{12} = 14.35 mm, d_{13} = 14.86 mm, d_{34} = 17.2 mm, d_{35} = 13.39 mm, d_{5L} = 15.17 mm, l_1 (length of resonator 1) = 20.28 mm, l_2 = 19.95 mm, l_3 = 24 mm, l_4 = 24.44 mm, l_5 = 22.39 mm. The minor axis of all elliptical irises is 6 mm and is fixed for the next two designs. The size of the filter is 57.7 mm × 31.4 mm × 24.44 mm and the volume are 1.91×10^4 mm^3. A similar filter designed using rectangular resonators would have a total length and volume of 71.10 mm and 2.41×10^4 mm^3, respectively, which are 23% longer and 26% bulkier.

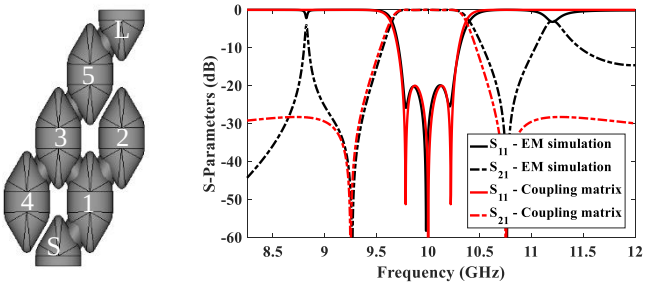

(a) (b)

Fig. 8. The wideband filter. (a) Layout. (b) EM simulation results compared with the responses from the coupling matrix.

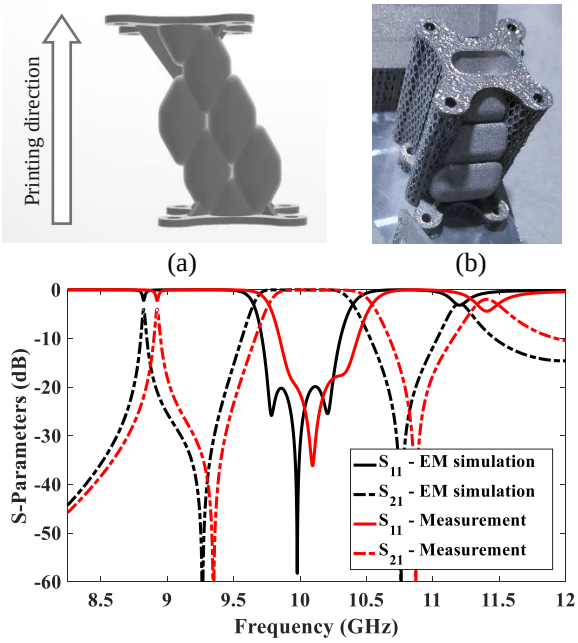

(a) (b)

(c)

Fig. 9. Wideband filter prototype. (a) Printing direction. (b) Fabricated filter on the printing platform. The net shape segments are supportive structures. (c) Measurement results compared with EM simulation.

The EM simulation of the filter compared with the coupling matrix response can be seen in Fig. 8(b). There are two spurious peaks out of band in the simulation. These are found to be strongly associated with the wide bandwidth of the filter. The strong coupling (and therefore large irises) allows resonances to establish at the lower and the upper bands. These are not seen in the narrow band filter to be presented later in Section III-B. Fig. 9(a) shows the printing direction of the wideband filter. This printing direction is adopted in the next two designs. An image of the printed structure on the printer substrate with external supporting structures is presented in Fig. 9(b). The tuning screw holes are drilled afterward. The thickness of the structure's outer walls and irises are set to 2 mm and 1 mm, respectively. The S-parameter of the filter, without tuning screws, has been measured and compared with the simulation in Fig. 9(c). The measurements show about 150 MHz frequency shift towards the higher frequency. Five M2 tuning screws have been added as can be seen in Fig. 10(a).

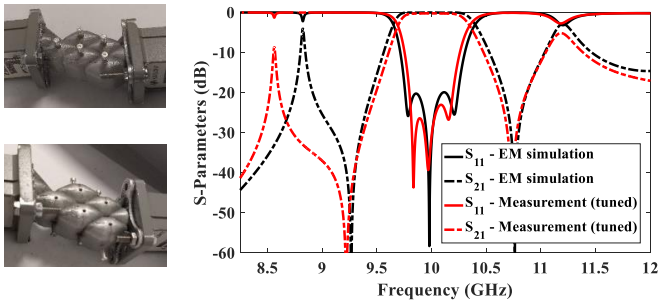

(a) (b)

Fig. 10. Wideband filter after tuning. (a) (Top) Tuning screws on the front wall. (Bottom) Same filter with tuning screws on the side walls. (b) Tuned results compared with EM simulation.

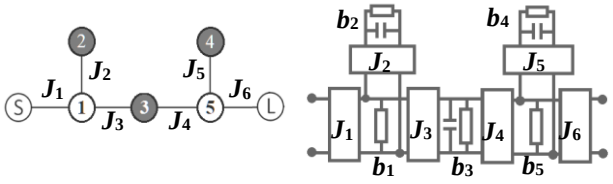

(a) (b)

Fig. 11. A third-order filter with two transmission zeros. (a) Topology. (b) Equivalent circuit model.

The tuning screws could also be implemented on the front walls (marked out in Fig. 3(a)) of the cavities. The side wall tuning screws are capable of correcting larger frequency shift whereas the front-wall tuning is more suitable for fine tuning. The latter is adopted in this design. The tuned response of the filter is compared with simulation in Fig. 10(b). The in-band insertion loss is measured 0.21 dB compared to the simulation, which is 0.16 dB. The simulation has been performed using the material effective conductivity, which is obtained using the nominal electrical conductivity and the surface roughness of the material. The filter bandwidth is reduced by 87 MHz compared to the simulation. The frequency of the lower out of band peak is reduced by almost 150 MHz. The achieved return loss is 23dB.

B. A third-order narrowband filter with two transmission zeros

The second design is another third-order filter with two TZs, but with a much smaller FBW of 1%. The TZs are at 9.85 GHz and 10.15 GHz. Fig. 11 shows the filter topology together with its equivalent circuit model. In order to demonstrate the capability of the resonator to implement various topologies the two dangling nodes are located at the first and last resonator rather than next to each other as in the first example.

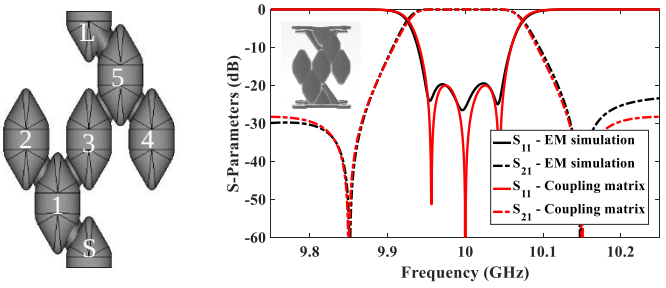

(a) (b)

Fig. 12. The narrowband filter. (a) Layout. (b) EM simulation results compared with those from the coupling matrix.

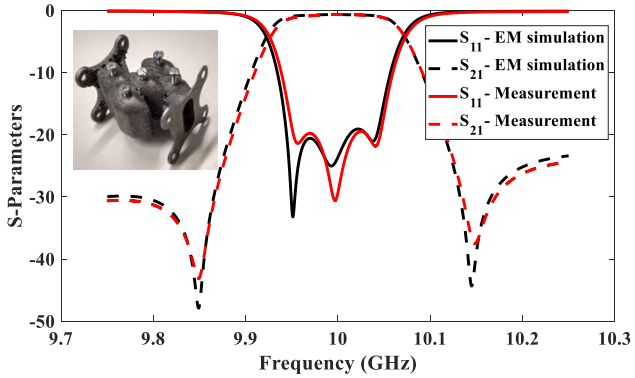

Fig. 13. Tuned results of the narrowband filter compared with EM simulation using effective conductivity of the A20X.

The same synthesis method has been used and the value of circuit elements in Fig. 11(b) are given as $J_1 = 1$, $J_2 = 2.5285$, $J_3 = 0.9700$, $J_4 = 1$, $J_5 = 2.6069$, $J_6 = 1.0310$, $b_1 = 2.329j$, $b_2 = 3j$, $b_3 = 0$, $b_4 = -2.4755j$ and $b_5 = -3j$. The coupling matrix of the filter is

$$\begin{bmatrix} 0.0000 & 1.0000 & 0.0000 & 0.0000 & 0.0000 & 0.0000 & 0.0000 \\ 1.0000 & 2.3290 & 2.5285 & 0.9700 & 0.0000 & 0.0000 & 0.0000 \\ 0.0000 & 2.5285 & 3.0000 & 0.0000 & 0.0000 & 0.0000 & 0.0000 \\ 0.0000 & 0.9700 & 0.0000 & 0.0000 & 1.0000 & 0.0000 & 0.0000 \\ 0.0000 & 0.0000 & 0.0000 & 1.0000 & -2.475 & 2.6069 & 1.0310 \\ 0.0000 & 0.0000 & 0.0000 & 0.0000 & 2.6069 & -3.000 & 0.0000 \\ 0.0000 & 0.0000 & 0.0000 & 0.0000 & 1.0310 & 0.0000 & 0.0000 \end{bmatrix} \quad (3)$$

Fig. 12(a) shows the filter structure, designed using the step-tuning method as the previous example. Five M3 tuning screws are located on the front wall of and halfway into each cavity. The dimensions of the filter are as follows: $d_{S1} = 13.87$ mm, $d_{12} = 12.2$ mm, $d_{13} = 9.69$ mm, $d_{35} = 9.05$ mm, $d_{34} = 12$ mm, $d_{5L} = 21.71$ mm, $l_1 = 20.6$ mm, $l_2 = 24.7$ mm, $l_3 = 26.17$ mm, $l_4 = 29.88$ mm, $l_5 = 26.85$ mm. The general dimension of the filter is 57.72 × 38.48 × 29.88 mm^3. The EM simulation results is compared

TABLE II
COMPARISON WITH PREVIOUSLY REPORTED FILTERS

Ref.	Cavity geometry	Printing direction	BW (MHz)	f_c (GHz)	IL (dB)	Q_u	Cond.	Tech.
T.W.	Hexagonal	Vertical	100	10	0.63	3400	A20X	SLM
[6]	Spherical	Vertical	500	8.2	<0.4	5700	A20X	SLM
[9]	Rectangular	45° tilted	10 GHz	90	1	NA	copper	MLS
[12]	super-ellipsoid	Lying down	250	14.1	<0.2	4600	silver	SLM
[13]	super-ellipsoid	Lying down	250	12.9	<1	4400	silver	SLM
[16]	Spherical	Vertical	54	11.5	1	5800	silver	SLM
[19]	Hexagonal	Vertical	500	13	0.58	1000	PLA	FDM

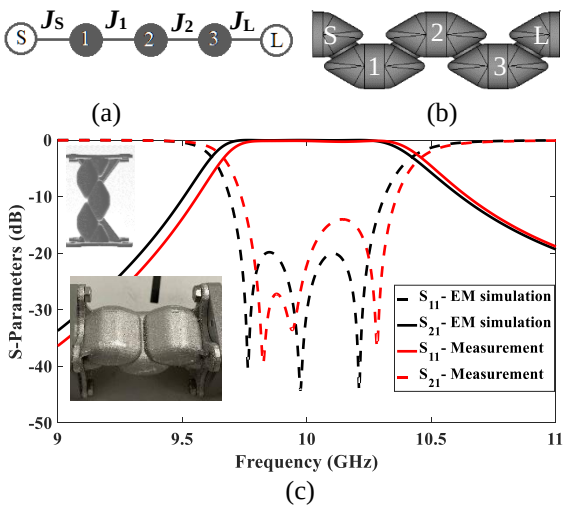

Fig. 14. (a) Filter topology. (b) Layout. (c) The measured results compared with the EM simulation.

with the coupling matrix in Fig. 12(b). The filter has been fabricated with the same thickness for walls and irises as the previous design. The tuned response is compared with simulation in Fig. 13, which shows an excellent agreement. The in-band insertion loss is measured as 0.63 dB, which is almost equal to the simulated loss of 0.65 dB. The fabricated filter is compared with other 3D printed filters reported in the literature in Table II. Different geometries have been used in designing filters in different frequency ranges. Each geometry offers different Q_u and printing direction. The spherical resonator filters have the highest Q_u and suitable for narrow-band filtering. The proposed filter made from hexagonal resonators with rounded corners shows a modest level of Q_u. The proposed hexagonal resonator is optimised for better surface finishing after 3D printing by minimising the ceiling surface compared with the spherical and ellipsoid resonators. Except for the rectangular resonator, the hexagonal, spherical, and ellipsoid resonators can offer more freedom in filter cavity arrangement. The resonators can be attached next or diagonal to each other. The proposed hexagonal resonator offers more compactness level compared to the other resonators by minimising the gap between cavities, when they sit next to each other.

C. A third-order wideband filter

The third example is a third-order filter, which is synthesised and designed using the well-known method in [22]. The specification of the filter is similar to the first design but without any TZs. The coupling matrix of the filter is given in (4). Fig. 14(a) shows the topology of the filter.

$$\begin{bmatrix} 0 & 1.0825 & 0 & 0 & 0 \\ 1.0825 & 0 & 1.0303 & 0 & 0 \\ 0 & 1.0303 & 0 & 1.0303 & 0 \\ 0 & 0 & 1.0303 & 0 & 1.0825 \\ 0 & 0 & 0 & 1.0825 & 0 \end{bmatrix} \quad (4)$$

The filter is designed as displayed in Fig. 14(b) with dimensions of l_1 = 24.81 mm, l_2 = 27.9 mm, l_3 = 24.79 mm, d_{S1}=14.3 mm, d_{12} = 9.97 mm, d_{23} = 9.96 mm, d_{3L} = 14.24 mm. The overall size of the filter is 56.24 mm × 17.24 mm × 27.9 mm and the volume is 1.44×10^4 mm^3. There are no tuning screws adopted in the design. A filter with similar specification using rectangular resonators Would have a total length and volume of around 78.26 mm and 1.72×10^4 mm^3, respectively, which are 28% longer and 15% bulkier. The S-parameter of the filter has been measured and compared with the simulation in Fig. 14(c), showing very good agreement without any tuning. The measurements show 52 MHz frequency shift towards the higher frequency. Simulation-based investigation shows that the frequency discrepancy could be because the length of resonators is around 300 µm less than the design. Moreover, there are some defected surfaces observed around the irises. This could also contribute to the frequency shifts. The in-band insertion loss is measured at 0.12 dB, while it is 0.15 dB in the simulation.

IV. Conclusion

A resonator structure, self-supportive for 3D printing, is presented to allow compact layout of coupled resonator filters with dangling nodes for generating TZs. The resonator provides a compact design compared to the regular rectangular resonators. For a resonator with a resonant frequency of 10 GHz, using the proposed resonator, the height of the structure is reduced by 36% compared with the rectangular resonator. The resonator offers a good modularity for the filter structure. The Q_u of the proposed resonator is 10% less than rectangular resonators. It has been shown that the Q_u can be improved by choosing a different θ_d, i.e., θ_d = 45˚ or mixed 30˚/45˚. Three different filters have been designed using the proposed resonator model and fabricated using SLM technology to verify the feasibility and capability of the resonator. The measurements show frequency shift after fabrication. This has been corrected by tuning. The side wall tuning is more suitable for the wideband filter, whilst the front wall tuning is effective for the narrow band filter.

References

[1] D. Miek, S. Simmich, F. Kamrath and M. Höft, "Additive Manufacturing of E-Plane Cut Dual-Mode X-Band Waveguide Filters With Mixed Topologies," in IEEE Transactions on Microwave Theory and Techniques, vol. 68, no. 6, pp. 2097-2107, June 2020, doi: 10.1109/TMTT.2020.2981057.

[2] K. Y. Chan, R. Ramer and R. Sorrentino, "Low-Cost Ku-Band Waveguide Devices Using 3-D Printing and Liquid Metal Filling," in IEEE Transactions on Microwave Theory and Techniques, vol. 66, no. 9, pp. 3993-4001, Sept. 2018, doi: 10.1109/TMTT.2018.2851573.

[3] I. Piekarz et al., "Wideband Microstrip to 3-D-Printed Air-Filled Waveguide Transition Using a Radiation Probe," in IEEE Microwave and Wireless Components Letters, vol. 32, no. 10, pp. 1179-1182, Oct. 2022, doi: 10.1109/LMWC.2022.3173407.

[4] A. Fontana et al., "A Novel Approach Toward the Integration of Fully 3-D Printed Surface-Mounted Microwave Ceramic Filters," in IEEE Transactions on Microwave Theory and Techniques, vol. 71, no. 9, pp. 3915-3928, Sept. 2023, doi: 10.1109/TMTT.2023.3267541.

[5] K. Zhao and D. Psychogiou, "Monolithic Multiband Coaxial Resonator-Based Bandpass Filter Using Stereolithography Apparatus (SLA) Manufacturing," in IEEE Transactions on Microwave Theory and Techniques, vol. 70, no. 9, pp. 4156-4166, Sept. 2022, doi: 10.1109/TMTT.2022.3193701.

[6] X. Wen et al., "SLM Printed Waveguide Dual-Mode Filters With Reduced Sensitivity to Fabrication Imperfections," in IEEE Microwave and Wireless

Components Letters, vol. 31, no. 11, pp. 1195-1198, Nov. 2021, doi: 10.1109/LMWC.2021.3096977.

[7] E. A. Rojas-Nastrucci, J. T. Nussbaum, N. B. Crane and T. M. Weller, "Ka-Band Characterization of Binder Jetting for 3-D Printing of Metallic Rectangular Waveguide Circuits and Antennas," in IEEE Transactions on Microwave Theory and Techniques, vol. 65, no. 9, pp. 3099-3108, Sept. 2017, doi: 10.1109/TMTT.2017.2730839.

[8] M. Baranowski, Ł. Balewski, A. Lamecki, M. Mrozowski and J. Galdeano, "The Design of Cavity Resonators and Microwave Filters Applying Shape Deformation Techniques," in IEEE Transactions on Microwave Theory and Techniques, vol. 71, no. 7, pp. 3065-3074, July 2023, doi: 10.1109/TMTT.2023.3239363.

[9] M. Salek et al., "W-Band Waveguide Bandpass Filters Fabricated by Micro Laser Sintering," in IEEE Transactions on Circuits and Systems II: Express Briefs, vol. 66, no. 1, pp. 61-65, Jan. 2019, doi: 10.1109/TCSII.2018.2824898.

[10] A. Mostaani et al., "Investigation of a 3D-Printed Narrowband Filter with Non-Resonating Nodes," 2021 IEEE MTT-S International Microwave Filter Workshop (IMFW), 2021, pp. 316-318, doi: 10.1109/IMFW49589.2021.9642309.

[11] Ameen, Wadea, Abdulrahman Al-Ahmari, and Muneer Khan Mohammed. "Self-supporting overhang structures produced by additive manufacturing through electron beam melting." The International Journal of Advanced Manufacturing Technology 104, no. 5 (2019): 2215-2232.

[12] P. Booth and E. V. Lluch, "Enhancing the Performance of Waveguide Filters Using Additive Manufacturing," in Proceedings of the IEEE, vol. 105, no. 4, pp. 613-619, April 2017, doi: 10.1109/JPROC.2016.2616494.

[13] P. Booth and E. V. Lluch. "Realising advanced waveguide bandpass filters using additive manufacturing." IET Microwaves, Antennas & Propagation 11, no. 14 (2017): 1943-1948.

[14] M. Simonelli, Y. Y. Tse, and C. Tuck. "Effect of the build orientation on the mechanical properties and fracture modes of SLM Ti–6Al–4V." Materials Science and Engineering: A 616 (2014): 1-11.

[15] F. Calignano, “Design optimization of supports for overhanging structures in aluminum and titanium alloys by selective laser melting”, Materials and Design, vol. 64, pp. 203-213, Dec. 2014.

[16] Qian, Lu, Yi Wang, Sheng Li, Abd El-Moez A. Mohamed, Moataz M. Attallah, Talal Skaik, Paul Booth, Laurent Pambaguian, César Miquel España, and Petronilo Martín-Iglesias. "A Narrowband 3-D Printed Invar Spherical Dual-Mode Filter With High Thermal Stability for OMUXs." IEEE Transactions on Microwave Theory and Techniques 70, no. 4 (2022): 2165-2173.

[17] Hameed, M., Xiao, G., & Xiong, C. (2018, May). Triple-mode wideband bandpass filter using triangular waveguide cavity. In 2018 IEEE MTT-S International Wireless Symposium (IWS) (pp. 1-3). IEEE.

[18] V. Weißmann, P. Drescher, H. Seitz, H. Hansmann, R. Bader, A. Seyfarth, A. Klinder, and A. Jonitz-Heincke. "Effects of build orientation on surface morphology and bone cell activity of additively manufactured Ti6Al4V specimens." Materials 11, no. 6 (2018): 915.

[19] K. Y. Chan, R. Ramer and R. Sorrentino, "Low-Cost Ku-Band Waveguide Devices Using 3-D Printing and Liquid Metal Filling," in IEEE Transactions on Microwave Theory and Techniques, vol. 66, no. 9, pp. 3993-4001, Sept. 2018, doi: 10.1109/TMTT.2018.2851573.

[20] R. J. Cameron, C. Kudsia and E. Mansour, “Microwave filters for communication systems,” 2nd ed., Hoboken, USA: J. Wiley., 2018, pp. 323–335.

[21] Amari, Smain, and Giuseppe Macchiarella. "Synthesis of inline filters with arbitrarily placed attenuation poles by using nonresonating nodes." IEEE Transactions on Microwave Theory and Techniques 53, no. 10 (2005): 3075-3081.

[22] J. S. Hong and M. J. Lancaster, Microstrip Filters for RF/Microwave Applications. New York, NY, USA: Wiley, 2001.